

Article

A Stable and Durable Triboelectric Nanogenerator for Speed Skating Land Training Monitoring

Zhuo Lu ¹, Zhenning Xie ², Yongsheng Zhu ², Changjun Jia ², Yao Zhang ¹, Jie Yang ¹, Junyi Zhou ³, Fengxin Sun ^{2,*} and Yupeng Mao ^{1,2,4,*} 

¹ School of Physical Education, Northeast Normal University, Changchun 130024, China

² Physical Education Department, Northeastern University, Shenyang 110819, China

³ Winter Sports Center, Hebei Sports Bureau, Shijiazhuang 050000, China

⁴ School of Strength and Conditioning Training, Beijing Sport University, Beijing 100084, China

* Correspondence: 2171435@stu.neu.edu.cn (F.S.); maoyupeng@pe.neu.edu.cn (Y.M.)

Abstract: In the current IoT era, the key to sports intelligence is the effective collection and analysis of sports data. Sports data can accurately reflect an athlete's athletic status and help coaches to develop competitive tactics and training programs. Wearable electronic devices used to collect sports data currently have several drawbacks, including their large size, heavy weight, complex wiring, high cost, and need for frequent power replacement. In this work, transparent polyamide-66 (PA-66) and transparent polytetrafluoroethylene (PTFE) films were used as friction layers, polydimethylsiloxane (PDMS) was used as a support layer, and conductive hydrogels were used as electrodes, which were simply combined to create stable and durable triboelectric nanogenerators (SD-TENG) with good mechanical and triboelectric properties. In the test, the output power was 1mW under a load resistance of 10MΩ. In addition, the integrated intelligent speed skating land training assistance system monitors the changes in the joints and joint chains of skaters during land training in real time. The successful demonstration of the use of SD-TENG in speed skating land training will help to promote the development and application of TENG in the fields of intelligent sport monitoring, smart wearable devices, and big data analysis.

Keywords: intelligent sport; wearable electronic devices; triboelectric nanogenerator; sport monitoring



Citation: Lu, Z.; Xie, Z.; Zhu, Y.; Jia, C.; Zhang, Y.; Yang, J.; Zhou, J.; Sun, F.; Mao, Y. A Stable and Durable Triboelectric Nanogenerator for Speed Skating Land Training Monitoring. *Electronics* **2022**, *11*, 3717. <https://doi.org/10.3390/electronics11223717>

Academic Editor: Enzo Pasquale Scilingo

Received: 18 October 2022

Accepted: 9 November 2022

Published: 13 November 2022

Publisher's Note: MDPI stays neutral with regard to jurisdictional claims in published maps and institutional affiliations.



Copyright: © 2022 by the authors. Licensee MDPI, Basel, Switzerland. This article is an open access article distributed under the terms and conditions of the Creative Commons Attribution (CC BY) license (<https://creativecommons.org/licenses/by/4.0/>).

1. Introduction

Intelligent sport monitoring has emerged as a key area of sport monitoring in the Internet of Things and big data era [1–8]. One purpose of this technology is to quantify athletes' motion behavior and kinematic patterns by utilizing wearable sensors to observe and recognize the motion features of the human body [9–19]. The main feature of speed skating is that its training cycle includes ice training and land training. The role of land training is to develop general and special physical qualities and to lay the physical and technical foundation for the training of the ice period. Therefore, the quality of land training directly affects the ice training quality. The monitoring methods currently used for speed skating land training are mainly based on high-speed cameras [20–23]. However, camera systems such as high-speed cameras have many limitations in terms of their practical applications. For example, a prototype computer vision system was designed to monitor driving status [24], but it is expensive and complex in design and relies on external power sources. A computer vision system with a parallel camera was designed to track the trajectory of athletes in short-track speed skating competitions [25], but the system is affected by its high cost, high power consumption, and high lighting requirements. A depth camera was proposed for human position detection [26], but this camera cannot achieve the recognition of human motion states, especially muscle and joint movements. Therefore, it is crucial to develop a simple, economical, lightweight, and portable self-powered wearable sensor for speed skating land training monitoring.

In the research on new energy development, economic and sustainable green energy has enthusiastically been adopted as a point of focus [27]. In 2012, Zhonglin Wang first proposed the concept of triboelectric nanogenerators (TENG) [28]. TENGs have shown many advantages, such as a low cost, easy fabrication, high power density, and a wide range of material choices, attracting the attention of many researchers [29–32]. They can collect and convert the low-frequency energy widely distributed in nature into electrical energy, which is an economic, green, and sustainable source of energy supply [33–37]. For example, scholars have designed and fabricated a solution-tube-based volume-effect nanogenerator for collecting energy from water waves [38]. Wave energy is known as a blue energy, and scholars have designed a fully symmetric triboelectric nanogenerator with an elliptical cylindrical structure to harvest blue energy [39]. To real-time measure wind speed and direction in environmental monitoring, scholars have designed an all-round wind-driven triboelectric nanogenerator [40]. In addition, TENG can be widely used as a self-powered sensor in sport, healthcare, health monitoring, and environmental monitoring, demonstrating an excellent sensitivity and stability [41–48]. However, there is a gap in the research on the use of TENG sensors to monitor speed skating land training. Therefore, in this work, we used TENG as a digital acquisition terminal and combined it with a host information processing system to achieve real-time motion evaluation. Based on the energy collection and self-powered sensing capabilities of the TENGs, we argue that it provides an effective method for monitoring speed skating land training.

In numerous studies on TENG, polytetrafluoroethylene (PTFE) and polyamide (nylon) have often been fabricated as friction layer materials in different ways. For example, a TENG with a highly nanostructured rough surface was obtained using porous PTFE membranes prepared by electrostatic spinning and polyamide-6 (PA-6) prepared by phase transformation [49]. A superhydrophobic TENG was obtained through fabrics with a polytetrafluoroethylene nanoparticle (PTFE NP) coating and polyamide (nylon) fabrics [50]. A washable TENG was obtained using polytetrafluoroethylene (PTFE) fabric and polyamide (nylon) fabric treated by the etching process [51]. Materials such as PTFE and nylon were chemically treated, doped, or process-treated, and although the electrical output performance of the TENG was improved, it increased the complexity and cost of the fabrication process.

Here, we present a simple and effective design for the fabrication of stable and durable triboelectric nanogenerators (SD-TENG) with excellent mechanical and frictional electrical properties. SD-TENG is formed of transparent polyamide-66 (PA-66) and polytetrafluoroethylene (PTFE) film as the friction layer, polydimethylsiloxane (PDMS) as the support layer, and hydrogel as the electrode. On the one hand, this simple method of producing TENGs simplifies the tedious and complicated production process and reduces the waste of chemical materials. On the other hand, it compensates for the defects of its high energy consumption, non-portability, and inaccuracy during the monitoring of the movement by the camera. The SD-TENG can be used as a biomechanical energy harvester and self-powered sensor in kinematic analysis. The SD-TENG also has the advantages of a small size (8 cm in length, 3 cm in width, and 0.3 cm in height), being lightweight (7.5 g), easy fabrication, and a low cost. In addition, the choice of hydrogel as an electrode improves the stability of the electrical output and prolongs the life of the device. Due to its excellent performance, SD-TENG was attached to the athletes' joints and real-time monitored the joints and joint chains of the skaters in land training. In addition, an intelligent speed skating land training assistance system was developed. The system used a computer to process the real-time data generated during land training and to accurately record and evaluate the completion of technical motions. The successful demonstration of the utility of SD-TENG for speed skating land training can not only promote the development of TENGs in biomechanical energy harvesting and sensing but also provide ideas for intelligent monitoring in competitive sport, self-powered systems in wearable smart devices, and big data analysis.

2. Experiment

2.1. Materials

PTFE film was obtained from Taizhou Huafu Plastic Industry Co., Ltd., Taizhou, China. The polyamide-66 (PA-66) film was obtained from Dongguan Yixuan Plastics Co., Ltd., Dongguan, China. N, N-dimethylformamide (DMF), deionized water, acrylamide (AM), lithium chloride (LiCl), N0, N0-methylene diacrylamide (MBA), ammonium persulfate (APS) and N0, N0, N0, N0-tetramethylethylenediamine (TLD) were obtained from Jintong Loctite, Beijing, China. DOW SYLGARD 184 part A (Base) and DOW SYLGARD 184 part B (curing agent) were purchased from Industrial Adhesives Superstore, Tianjin, China.

2.2. Fabrication of SD-TENG

The preparation of the PDMS support layer: Firstly, DOW SYLGARD 184 Part A (Base) and DOW SYLGARD 184 Part B (Curing Agent) were thoroughly mixed in a 10:1 weight ratio to obtain the PDMS pre-solution. Secondly, the mixed solution was poured into the mold and heated for 20 min at 85 °C using a thermostatic heater. Finally, PDMS support layers were obtained from the cured PDMS that was removed from the mold.

The preparation of hydrogel electrodes: The monomer was AM, the cross-linking agent was MBA, the initiator was APS, and the catalyst was TMED. Firstly, deionized water in a quantity of 40 mL was weighed and stirred at 800 rpm with a magnetic stirrer. A total of 12 g of acrylamide powder, 14 g of lithium chloride particles, 0.003 g of ammonium persulfate, and 0.0025 g of N0, N0-methylene diacrylamide, were weighed successively and added to the stirred deionized water in turn and stirred until the drug particles were completely dissolved to obtain the hydrogel pre-solution. Finally, the pre-solution was poured into the mold and TMEDA was added to speed up the integration of the hydrogel to create PAAM-LiCl hydrogel.

Fabrication of SD-TENG sensors: First, we cut out a PA-66 film and PTFE film of the same size according to the size of the support layer. Secondly, the cut PA-66 film and PTFE film were applied to the top and bottom surfaces of the PDMS support layer, respectively. Finally, we cut two pieces of hydrogel electrode sheets of a suitable size to fit the PA-66 film and PTFE film, respectively, and fixed them with tape at both ends of the device.

2.3. Characterization and Measurement

To simulate joint motion, the SD-TENG was mounted on a stepper motor. Different stepping distances and frequencies of the stepper motor were established to test the performance of the SD-TENG. The SD-TENG generated waveform signals that were recorded by an oscilloscope (Shenzhen sto1102c, Shenzhen, China). The data transmission and reception were realized using the AD wireless transmission module (the photo and single-line diagram of the AD wireless transmission module are shown in Figures S1 and S2). The data processing was performed by the computer.

3. Results and Discussion

The speed skating training period differs from that of track and field sports in that it has unique ice and non-ice training periods. In the non-ice training cycle, land-based simulated ice training is the main focus. The efficiency of the training is determined by whether the land training matches the ice sport technique or not. Therefore, an accurate and reliable assessment of the stability, frequency of change, and extension of the athlete's joints during land-based training are required. Here, we fabricated a stable and durable triboelectric nanogenerator (SD-TENG) through an easy method. The SD-TENG can record the athletes' motion data in real time and present it as an electrical signal. Based on the output signal of the SD-TENG, the coach can adjust the technical movements of the athletes and develop a training plan suitable for the athletes, thus scientifically and systematically improving the efficiency of the athletes' land training. Figure 1a demonstrates the imitation exercise of a belt traction bend in land training, and the SD-TENG can be attached to the ankle, knee, and hip joints of athletes. The joint movement causes the SD-TENG to

deform, and the two friction layers generate an electrical output based on the frictional and electrostatic induction effects. Based on this, the SD-TENG achieves biomechanical energy harvesting and self-powered sensing. Figure 1b shows the application of SD-TENG as an energy source and data source in smart sports training. The mechanical energy generated by the athlete when performing the training movements is collected and converted into electrical energy by SD-TENG, and the changes in joint status are recorded by SD-TENG. The motion information collected and recorded by SD-TENG continuously injects new data for the sports big data analysis, gradually realizing the intelligent development of the information collection, transmission, and processing analysis. Figure 1c shows the manufacturing process of SD-TENG. First, in a certain ratio, acrylamide, lithium chloride, ammonium persulfate, and NN methylenebisacrylamide were mixed, and the drugs were fully dissolved and poured into the mold, and rapid molding was initiated by adding a drop of TMEDA catalyst. A hydrogel electrode with stretching capabilities was created, and Figure S3 depicts the stretching test. Following the mixture of the PDMS solution with a curing agent at a 10:1 weight ratio, the mixture was poured into the mold and dried at 85 °C for 20 min. Finally, the polyamide-66 (PA-66) film, PDMS support layer, and polytetrafluoroethylene (PTFE) film were stacked sequentially in the order of top, middle, and bottom, respectively, and the top and bottom surfaces were covered with the hydrogel electrodes to obtain the complete SD-TENG. To assess the performance of the simply fabricated SD-TENG, a brief comparison was performed using TENGs from similar works by other researchers (Table 1). Although the friction layer materials in these two works were obtained in different ways, the TENGs are close in their electrical output performance. Figure 1d shows the optical image of the complete device with good transparency. Figure 1e demonstrates the soft bendability of the device, showing that the device is comfortable when attached to the joint and avoids interference with normal training.

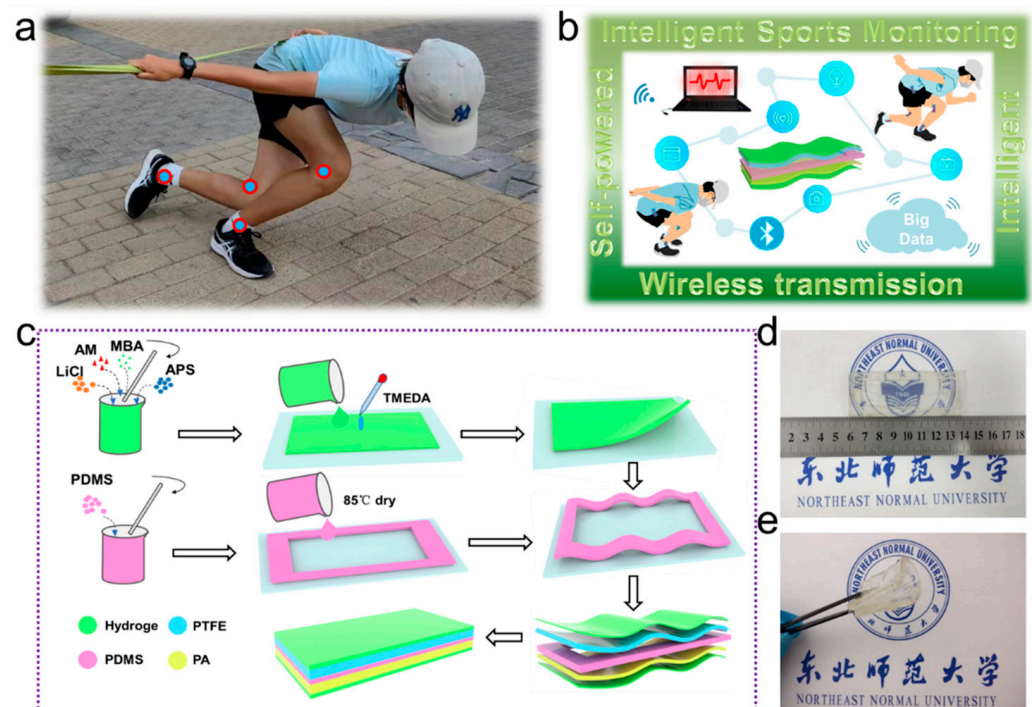


Figure 1. Application scenarios and production process of SD-TENG. (a) Application of SD-TENG in speed skating land training. (b) Application of SD-TENG in smart sports monitoring. (c) The fabrication process of SD-TENG. (d) The optical photograph of SD-TENG. (e) The photograph of SD-TENG's flexible display.

Table 1. Comparison of friction layer materials.

	Mode	Materials	Frictional Contact Area (cm ²)	Open Circuit Voltage at 2.4 Hz (V)	V/cm ²
This work	Contact separation mode	PA-66(Nylon) film/PTFE film	6 × 1.5	64	7.1
Other work [51]	Contact separation mode	Nylon fabric/PTFE fabric	5 × 5	190	7.6

A diagram of SD-TENG's working mechanism can be found in Figure 2a. When SD-TENG is fully squeezed by an external force, PA-66 is in complete contact with PTFE, and charge transfer occurs at the interface between PA-66 and PTFE due to their different electronegativities (Figure 2(aI)). Since the surface electron affinity of PTFE is higher than that of PA-66, electrons are transferred from the PA-66 surface to the PTFE surface, presenting PA-66 with a positive charge and PTFE with an equal amount of negative charge. When the external pressure disappears, PA-66 and PTFE gradually separate, and electrons are transferred from the bottom electrode to the top electrode through an external circuit under the action of electrostatic force (Figure 2(aII)). When the pressure disappears completely, as shown in Figure 2(aIII), SD-TENG reaches the equilibrium state, and no further transfer of electrons occurs. When the external pressure is reapplied, electrons are transferred from the top electrode to the bottom electrode through the external circuit due to the electrostatic force (Figure 2(aIV)). When full contact is made again, the two friction layer charges are balanced again, and one cycle is completed. Thus, an alternating current is generated when the PA-66 film is periodically separated from the PTFE film. As shown in Figure 2b, the potential distributions of the four operating states of SD-TENG are simulated accordingly using COMSOL. In Figure 2c, the voltage signal for the SD-TENG switch polarity test is demonstrated. Different voltage waveforms are generated by pressing and releasing the SD-TENG in the forward and reverse states, which indicates that the voltage signal originates from the sensor rather than the measurement system. Based on this unique periodic operating mechanism of SD-TENG and the periodic characteristics exhibited by the motion match, it can effectively be applied to the monitoring of various motions.

The human body has a complex motion system, but the most basic form of motion is the rotation of the skeleton around a joint through the power provided by the muscles. The cooperation of bones and muscles produces a variety of motion forms, and the SD-TENG, as a sensor for monitoring motion, needs to ensure that the sensor can meet the needs of various movements. A preliminary test of the SD-TENG's electrical performance was conducted before it was put to practical use. As shown in Figure 3, we fixed the SD-TENG, with a size of 8 × 3 cm and a friction contact area of 6 × 1.5 cm², to a stepper motor and simulated the joint motion process using the stepper motor. Figure 3a shows the output voltage of the SD-TENG for the same bending angle, the same force, and different frequency conditions. The output voltage of the SD-TENG remained consistent at 64 V under low-frequency (1 Hz, 2 Hz, 3 Hz, and 4 Hz) conditions. The reason for the consistent output voltage is that the low frequency does not lead to the accumulation of triboelectric charges. It also indicates that the SD-TENG has the stability required to monitor low-frequency motions. The SD-TENG output current is shown in Figure S4. The output current was maintained at 5 μA at low frequencies (1 Hz, 2 Hz, 3 Hz, and 4 Hz) and a 2 MΩ load, which indicates that the SD-TENG also has current output stability. For speed skating land training, the fast and variable joint angles require a device with stable output for monitoring, and the SD-TENG can well meet the needs of land training monitoring. SD-TENG's responses at different frequencies are shown in Figure 3b, and they were derived using the following equation:

$$R\% = \left| \frac{V_0 - V_i}{V_i} \right| \times 100\% \quad (1)$$

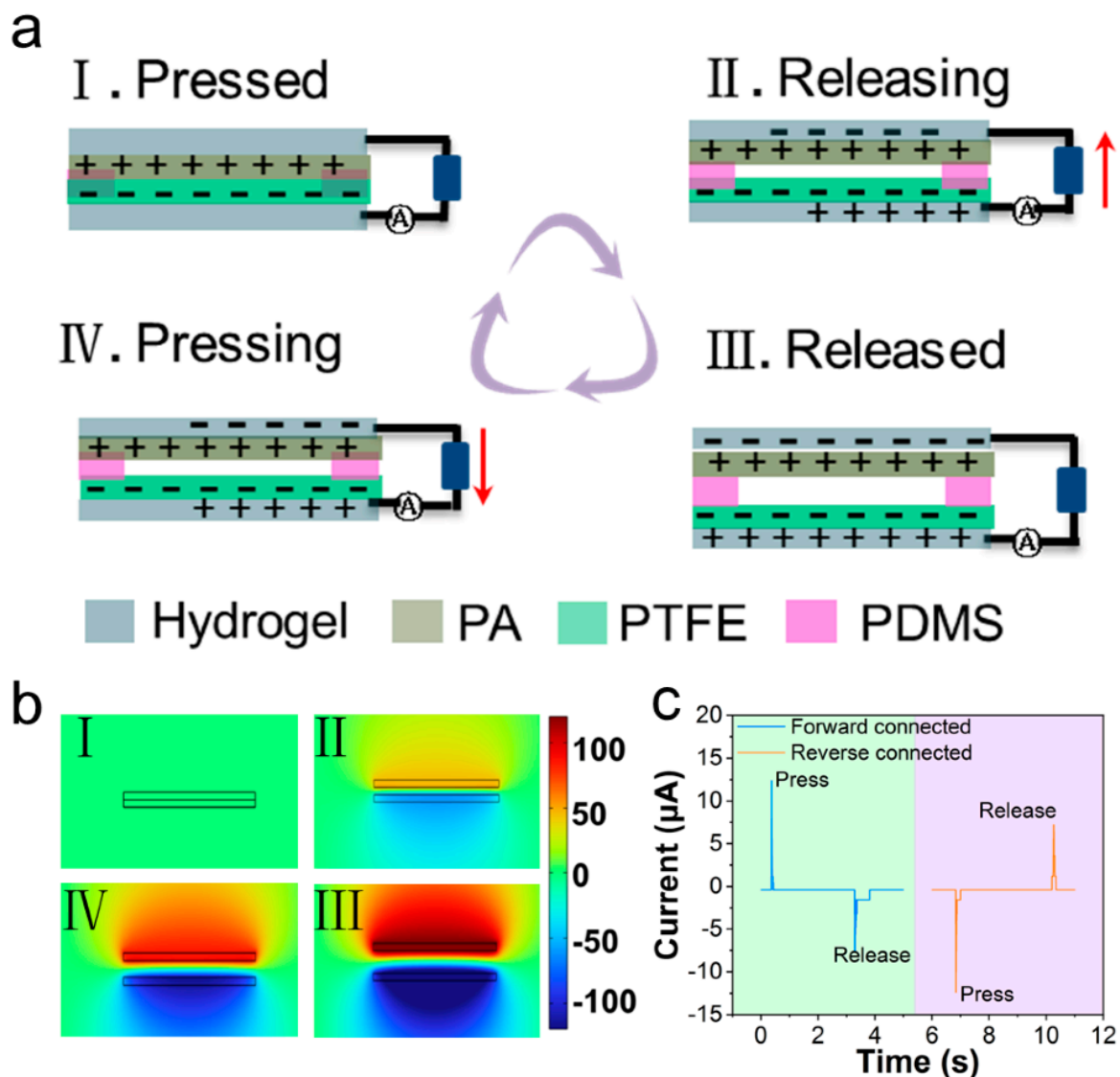


Figure 2. The SD-TENG mechanism. (a) Schematics of the operating principle of the SD-TENG. (b) COMSOL simulations were performed to clarify SD-TENG's working principle. (c) Switching polarity test of SD-TENG.

Here, V_0 and V_i are the output voltages at a frequency of 1 Hz and at another frequency of Hz, respectively. When the frequency is 1, 2, 3, and 4 Hz, the response of SD-TENG is 0, 0, 0, and 0%, respectively. Similarly, the current responses of the SD-TENG were tested at low frequencies (1 Hz, 2 Hz, 3 Hz, and 4 Hz) and at 2 MΩ loads, with a response of 0% (Supplementary Information Figure S5). These data indicate that the SD-TENG has superb stability for human joint motion monitoring. The SD-TENG can sensitively and accurately monitor the changes in human joint motion during a fast-paced speed skating event with frequent changes in the joint angles. Figure 3c shows the output voltage at different bending angles with the same frequency (4Hz). When the bending angle is 4.05°, 6.08°, 8.12°, and 10.17°, the frictional electric output voltage is 21, 26, 36, and 43 volts, respectively. The output current of the SD-TENG was measured immediately after adding a 2 MΩ load under the same conditions, as shown in Figure S6. SD-TENG can accurately calculate the change in the angle by the change in the output voltage, through which coaches can finely grasp the change in the angle of each joint of the athlete's body. The linear relationship between the bending angle and output voltage of SD-TENG is shown in Figure 3d. The formula is:

$$V \approx 5.02 + 3.72 \times \text{degree} \quad (2)$$

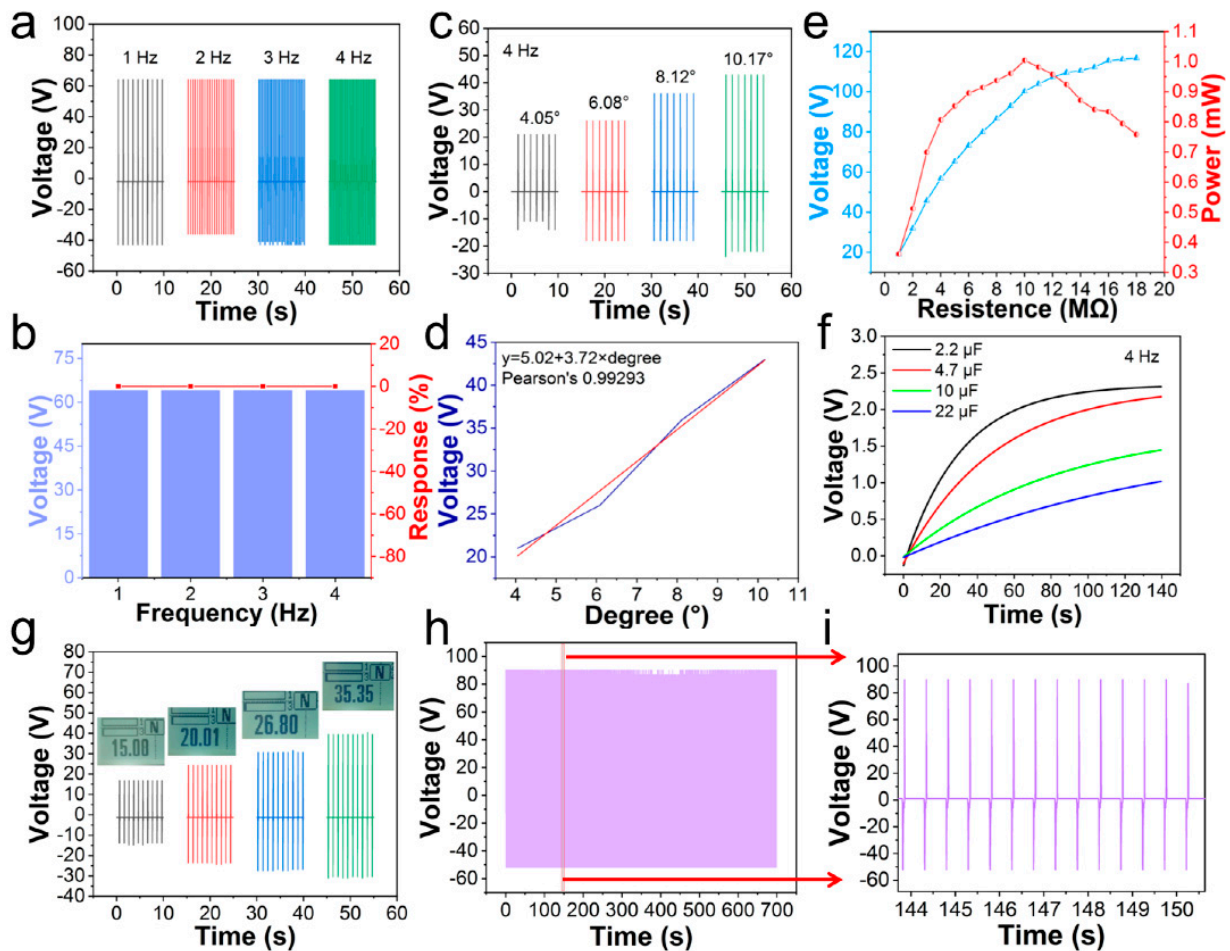


Figure 3. The electrical output performance of SD-TENG. (a) Relationship between the frequency and output voltage of SD-TENG for the same bending angle. (b) The voltage responses of SD-TENG at different frequencies. (c) Relationship between the angle and output voltage of SD-TENG at the same frequency. (d) Linear fit between the output voltage and bending angle of SD-TENG at the same frequency. (e) The voltage and power of SD-TENG under different load resistances. (f) The SD-TENG charging the 2.2 μF , 4.7 μF , 10 μF and 22 μF capacitors. (g) The test of the SD-TENG response to force. (h) The stability test of SD-TENG. (i) Details of the stability test.

In this study, the angle and voltage are significantly correlated with each other, as indicated by their Pearson correlation coefficient of 0.99293. A comparison of SD-TENG's output voltage and output power with different load resistances is shown in Figure 3e. It can be seen from Figure 3e that the output voltage increases as the load resistance increases, and the power of SD-TENG has a maximum value of 1.004 mW at the load resistance of 10 M Ω ; thus, it is known that the resistance of SD-TENG is 10 M Ω . SD-TENG's power density can be calculated as 0.112 mW/cm² due to the 9 cm² contact area of the frictional electrical parts. Figure 3f shows the SD-TENG charging its different capacitors. When the frequency is 4 Hz, the SD-TENG charges the 2.2 μF , 4.7 μF , 10 μF , and 22 μF capacitors for 140 s to 2.31 V, 2.18 V, 1.45 V, and 1.02 V, respectively. By converting the mechanical energy of human movement into electrical energy, SD-TENG can be used both as a sensor and as an energy collector. To explore the effect of temperature on the SD-TENG, we conducted a thermal stability test, as shown in Figure S7. The average output voltages were 64.4 V, 66.4 V, 66.4 V, and 68.8 V. The human skin temperature is always maintained at 36–37 °C, and the SD-TENG, as a sensor attached to the human skin, shows an excellent thermal stability. Figure 3g shows the response of the SD-TENG to the force. When the force was 15 N, 20.1 N, 26.8 N, and 35.35 N, the output voltage of SD-TENG was 16.8 V, 24.4 V, 30.8 V, and 39.6 V, respectively. The relationship between the output voltage and force is shown

in Figure S8. When the bending angle was certain, the output voltage increased with the increase in the force. This characteristic can accurately reflect the change on the athlete's force in speed skating land training. Figure 3h shows the stability test of the SD-TENG. After 700 s of the stability test, the SD-TENG still maintained a stable output, which can ensure the continuous and uninterrupted monitoring of athletes in long-distance speed skating programs. Figure 3i is a detailed schematic of the stability test, showing that the sensor is stable in long-term operation and guarantees the accuracy of the data transmission. In addition to stability, the durability of the device over a long period of time determines the service life, and for this reason, we tested the durability of the device. In Figure S9, the durability test of SD-TENG is demonstrated. At the same frequency and angle, the output voltage of SD-TENG was reduced from 90 V to 77 V after 30 days. The reason for the reduction in the output voltage may be due to the water loss of the hydrogel electrode. Although there is a reduction in the voltage output, the reduced output voltage still meets the needs of our work.

SD-TENG can be used both as a sensor for monitoring changes in human joints and as an energy harvesting device. The conversion and storage of mechanical energy into electrical energy can be used for selective utilization, thus further improving the efficiency of the SD-TENG. The SD-TENG equivalent circuit diagram is shown in Figure 4a and includes a capacitor, a bridge, and a load. The SD-TENG can switch between the charging and discharging modes. As shown in Figure 4b, the electrical energy generated by a simple tap of the SD-TENG can easily light up 124 LEDs (Supplementary Video S1), which further demonstrates that the SD-TENG can convert mechanical energy into electrical energy to continuously power the device. Furthermore, we investigated the energy conversion efficiency of the SD-TENG. Energy conversion efficiency is defined as the ratio of the available energy output from an energy conversion device relative to its input energy. The energy conversion efficiency equation is as follows:

$$\eta = \frac{E_{ele}}{W_{total}} \times 100\% = \frac{\int I^2 R dt}{E_k} \times 100\% \quad (3)$$

where E_{ele} and W_{total} are the electrical energy transferred to the load and the total energy acting on the sensor, respectively, and E_k is the kinetic energy of the mechanical rod arm. E_{ele} at a load of 10 M Ω is demonstrated in Figure S10. The energy conversion efficiency is calculated to be 0.078% using the equation. Figure 4c,d shows the actual charging and discharging of a calculator and an electronic watch, respectively (Supplementary Video S2). First, one taps the SD-TENG to charge the capacitor for a period of time and then turns on the switch to power the calculator and the electronic watch. As shown in Figure 4c,d, the electronic calculator and the watch successfully lit up in the tests. These demonstrations all show that SD-TENG has great potential for sustainable clean energy applications.

Speed skating land exercise, also known as land imitation exercise, is an indispensable basic exercise method. Reasonable and effective land exercises can not only lay a good foundation for athletes but also improve the physical qualities related to speed skating. In the training process, according to the technical characteristics of the ice and target muscle groups to be trained, land training movements are designed. Examples include the performance side stirrups and bent knee walk exercises in straight road land training and belt traction bend imitation exercises in road bend training. In this work, our main focus was the monitoring of side stirrup training and belt traction training in land training. Figure 5a shows the output voltage of the knee flexion during the side stirrup exercise performed by two athletes. By comparing the output voltage plots of the two athletes, it can be seen that the output voltage curve of Athlete 1 is smoother than the output voltage curve of Athlete 2. The smoother the curve is, the better the stability of the athlete's knee joint is. In the high-speed gliding state, the knee joint stabilization ensures a low center of gravity of the body, which contributes to the reduction in wind resistance. Figure 5b shows the output voltage of the ankle joint angle change during the side stirrup exercise performed by the two athletes. By comparing the output voltage graphs of the two athletes, it can be

seen that the low peak of the output voltage curve of Athlete 1 is in front of the high peak. This is caused by a different movement of the ankle joint. In speed skating ice training, when an athlete wearing a skate completes a side stirrup movement, the side stirrup foot is stretched out in parallel until the knee is fully extended. Afterward, due to the fact that the blade of the clap ice skate can be separated from the heel of the skate, the athlete’s side stirrup foot undergoes a plantarflexion process, in which the athlete can obtain a continuous propulsive force. The output voltage graph for Athlete 2 has a low peak in front of the high peak, indicating that Athlete 2 has plantarflexion of the skating foot before the knee joint is fully extended. The intuitive impact of this occurrence on the ice is poor skating and a slow speed improvement. Assistance simulation training occupies an important place in sports training, as it can help athletes to master the technical movements by reducing the difficulty of the sport, and help them the motor skills to develop from the generalization stage to the automation stage. Figure 5c shows the voltage output of the knee joint bending angle change during the belt traction imitation exercise for the two athletes. Athletes require great leg strength to overcome the centrifugal forces during cornering on ice. Thus, the more explosive the athlete’s legs are, the faster the rate of the knee stirrups and extensions will be, demonstrating fast and stable cornering during the sport. Therefore, it is necessary to monitor the changes in the size and frequency of the knee joint angle during belt traction training. From Figure 5c, it can be seen that Athlete 1 completed the movement more times and with a greater amplitude than Athlete 2 in the same timeframe, indicating that Athlete 1 completed the bending simulation training with a fast frequency and full extension of the knee joint. Athlete 2 was slightly worse than Athlete 1. Therefore, the strength training of the leg muscles and ankle spreader muscles should be strengthened during the training. Figure 5d shows the operation mode of the SD-TENG-based wireless intelligent land-assisted training system. In land training, the SD-TENG is attached to the ankle and knee joints of the athlete, and the device detects and collects motion data when the angles of the ankle and knee joints change. The acquired motion data are transmitted wirelessly through the system’s transmitter to the data receiver and processed by the computer in real time, and finally, the athletes’ movement performance quality is rated in real time in the form of a visual interface (Supplementary Video S3). The combination of SD-TENG as a data source and the wireless intelligent land-assisted training system provides a reliable guarantee of the quality of speed skating land training.

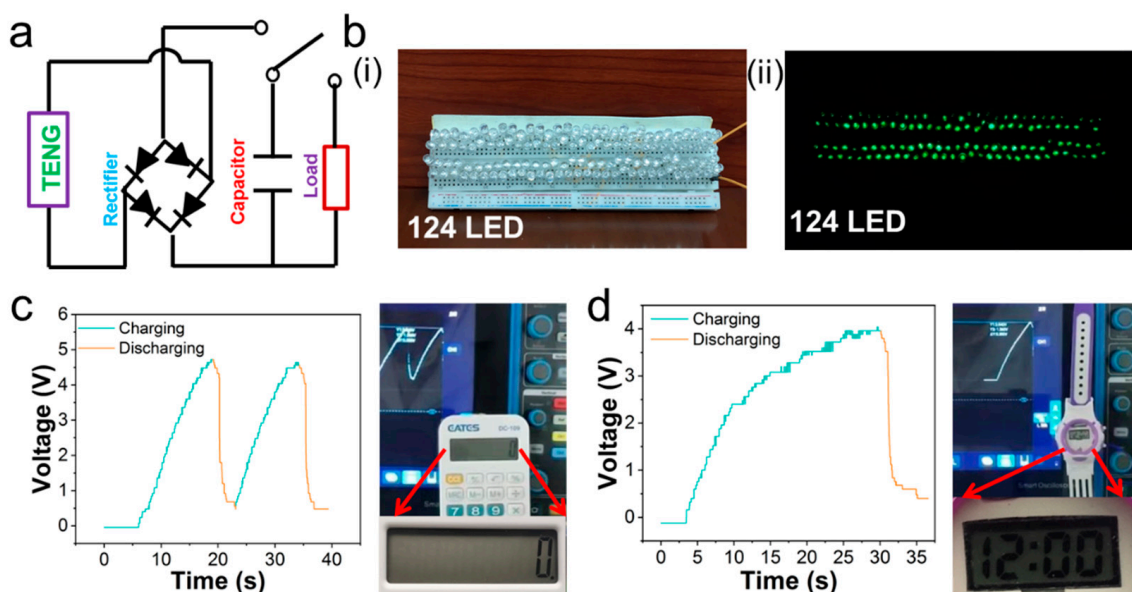


Figure 4. Power supply performance test of SD-TENG. (a) Equivalent circuit diagram of SD-TENG for charging and discharging. (b) The SD-TENG is used as a power supply to light up 124 green LEDs. (c) The SD-TENG charges a calculator. (d) The charging of an electronic watch.

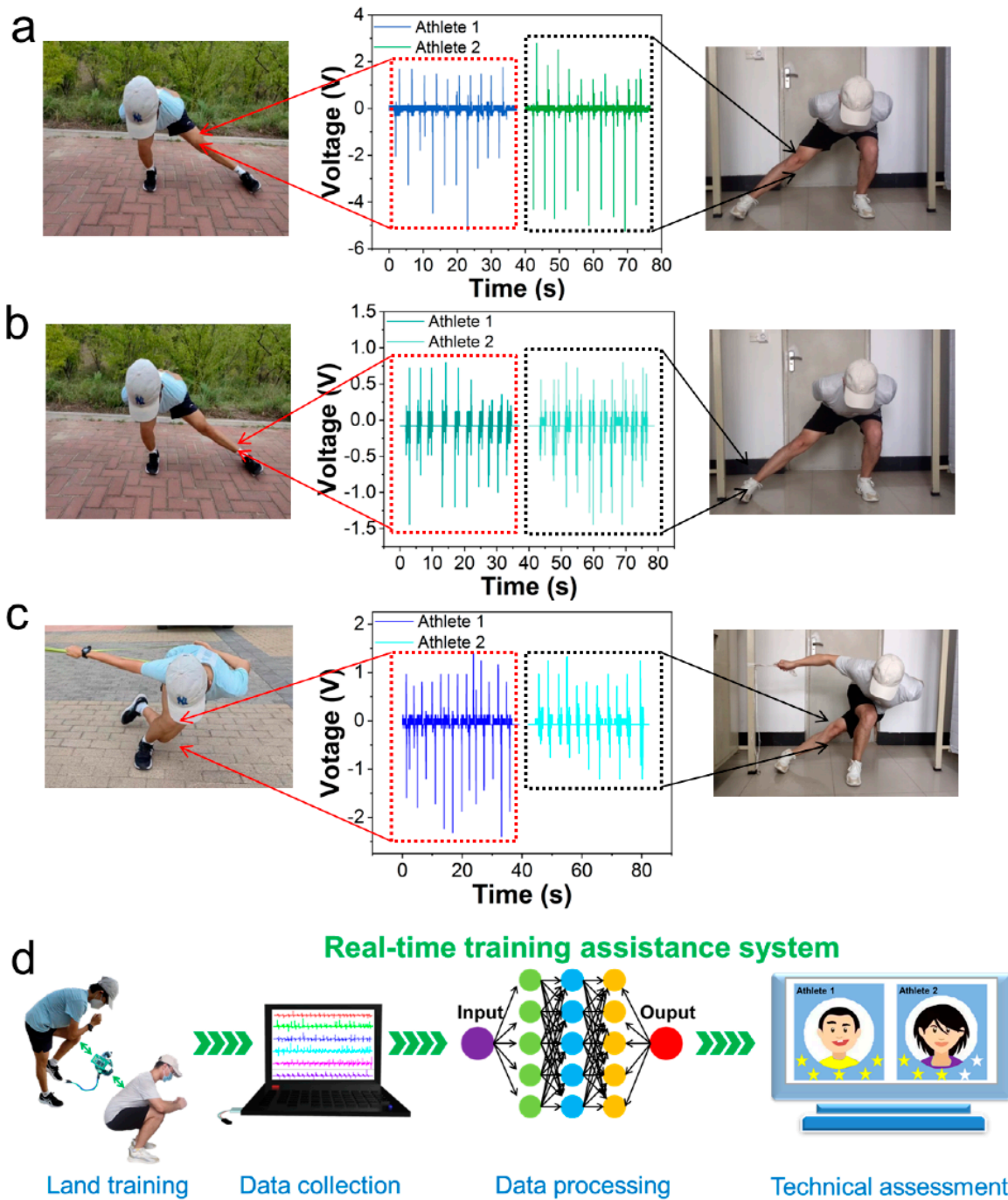


Figure 5. Application of SD-TENG in land training (a) Knee output voltage diagram of land training side stirrup exercise. (b) Ankle output voltage diagram of land training side stirrup exercise. (c) Knee joint output voltage diagram of the belt traction simulation training. (d) The operating diagram of the speed skating land training assistance system.

4. Conclusions

In summary, the SD-TENG self-powered sensor designed in this study provides a simple and easy method for the land-assisted training monitoring of speed skaters. It uses transparent polyamide-66 (PA-66) and polytetrafluoroethylene (PTFE) films as the friction layer, flexible polydimethylsiloxane (PDMS) as the support layer, and conductive hydrogel as the electrode. Due to its excellent performance, SD-TENG can be applied to the ankle, knee, and hip joints of athletes. The joint movement causes the SD-TENG to deform, and the two friction layers generate electrical outputs based on the frictional and

electrostatic induction effects, which finally realizes the real-time monitoring of the joints and joint chains of the skaters in land training. SD-TENG can be used as a data source to collect real-time data generated during land training, which is then inputted into the intelligent speed skating land training assistance system for data processing to accurately record and evaluate the completion of technical movements and, finally, to display the evaluation results on the terminal device. The evaluation results help coaches and athletes to understand the quality of movement techniques in real time so that they can improve the movements over time. This research opens up greater possibilities for sustainable energy collection and storage devices and the development of intelligent wearable devices. At the same time, the digitization of sports training is of great importance for the development of sports.

Supplementary Materials: The following supporting information can be downloaded at: <https://www.mdpi.com/article/10.3390/electronics11223717/s1>, Figure S1. AD wireless transmission module. Figure S2. The single-line diagram of the AD wireless transmission module. Figure S3. Hydrogel electrode stretchability test. Figure S4. SD-TENG output current at the same angle with different frequencies when the external load is 2 M Ω . Figure S5. The current and response of SD-TENG at different frequencies. Figure S6. SD-TENG output current at the same frequency with different angles when the external load is 2 M Ω . Figure S7. Thermal stability test of SD-TENG. Figure S8. The relationship diagram between the output voltage and force of SD-TENG. Figure S9. The durability test of the SD-TENG. Figure S10. The output current of SD-TENG with a load resistance of 10 M Ω . Video S1: The SD-TENG spotlight test; Video S2: The SD-TENG charges the electronic calculator and electronic watch; Video S3: Display of the speed skating land training real-time training assistance system.

Author Contributions: The manuscript was written through the contributions of all the authors. Conceptualization, Z.L. and Y.M.; methodology, Z.X., J.Z. and Y.Z. (Yongsheng Zhu); software, C.J.; validation, Y.Z. (Yao Zhang) and J.Y.; writing—original draft preparation, Z.L.; writing—review and editing, F.S. and Y.M. All authors have read and agreed to the published version of the manuscript.

Funding: Winter Sports Training monitoring technical services, 2020021300002.

Informed Consent Statement: Informed consent was obtained from all subjects involved in the study.

Data Availability Statement: The data presented in this study are available on request from the corresponding author.

Conflicts of Interest: The authors declare no conflict of interest.

References

1. Wang, F.; Huang, Q. Construction and Evaluation of Sports Rehabilitation Training Model under Intelligent Health Monitoring. *Wirel Commun. Mob. Com.* **2022**, *2022*, 9439076. [[CrossRef](#)]
2. Chen, H.; Lu, Q.; Cao, X.; Wang, N.; Wang, Z. Natural polymers based triboelectric nanogenerator for harvesting biomechanical energy and monitoring human motion. *Nano Res.* **2022**, *15*, 2505–2511. [[CrossRef](#)]
3. Gao, Q.; Cheng, T.; Wang, Z.L. Triboelectric mechanical sensors—Progress and prospects. *Extrem. Mech. Lett.* **2021**, *42*, 101100. [[CrossRef](#)]
4. Mao, Y.; Zhu, Y.; Zhao, T.; Jia, C.; Wang, X.; Wang, Q. Portable Mobile Gait Monitor System Based on Triboelectric Nanogenerator for Monitoring Gait and Powering Electronics. *Energies* **2021**, *14*, 4996. [[CrossRef](#)]
5. Ren, L. A triboelectric nanogenerator based on foam for human motion posture monitoring. *Mater. Technol.* **2022**, *37*, 1140–1145. [[CrossRef](#)]
6. Song, Z.; Zhang, X.; Wang, Z.; Ren, T.; Long, W.; Cheng, T.; Wang, Z.L. Nonintrinsic Monitoring of Droplet Motion State via Liquid-Solid Contact Electrification. *ACS Nano* **2021**, *15*, 18557–18565. [[CrossRef](#)] [[PubMed](#)]
7. Sun, P.; Cai, N.; Zhong, X.; Zhao, X.; Zhang, L.; Jiang, S. Facile monitoring for human motion on fireground by using MiEs-TENG sensor. *Nano Energy* **2021**, *89*, 106492. [[CrossRef](#)]
8. Zhang, X.; Gao, Q.; Gao, Q.; Yu, X.; Cheng, T.; Wang, Z.L. Triboelectric Rotary Motion Sensor for Industrial-Grade Speed and Angle Monitoring. *Sensors* **2021**, *21*, 1713. [[CrossRef](#)]
9. Chung, S.; Lim, J.; Noh, K.J.; Kim, G.; Jeong, H. Sensor Data Acquisition and Multimodal Sensor Fusion for Human Activity Recognition Using Deep Learning. *Sensors* **2019**, *19*, 1716. [[CrossRef](#)] [[PubMed](#)]
10. Luo, Z.; Duan, J.; Xu, H.; Wang, Y.; Liu, J.; Yao, X.; Zhang, B. Flexible Capacitive Pressure Sensor Based on an Embedded Rib Fabric with a Bionic Sloping Petal Structure. *IEEE Sens. J.* **2021**, *21*, 20119–20128. [[CrossRef](#)]

11. Xie, L.; Chen, P.; Chen, S.; Yu, K.; Sun, H. Low-Cost and Highly Sensitive Wearable Sensor Based on Napkin for Health Monitoring. *Sensors* **2019**, *19*, 3427. [[CrossRef](#)] [[PubMed](#)]
12. Cheng, Y.; Wang, K.; Xu, H.; Li, T.; Jin, Q.; Cui, D. Recent developments in sensors for wearable device applications. *Anal. Bioanal. Chem.* **2021**, *413*, 6037–6057. [[CrossRef](#)] [[PubMed](#)]
13. Chun, S.; Son, W.; Kim, D.W.; Lee, J.; Min, H.; Jung, H.; Kwon, D.; Kim, A.H.; Kim, Y.-J.; Lim, S.K.; et al. Water-Resistant and Skin-Adhesive Wearable Electronics Using Graphene Fabric Sensor with Octopus-Inspired Microsuckers. *ACS Appl. Mater. Inter.* **2019**, *11*, 16951–16957. [[CrossRef](#)] [[PubMed](#)]
14. Khoshmanesh, F.; Thurgood, P.; Pirogova, E.; Nahavandi, S.; Baratchi, S. Wearable sensors: At the frontier of personalised health monitoring, smart prosthetics and assistive technologies. *Biosens. Bioelectron.* **2021**, *176*, 112946. [[CrossRef](#)] [[PubMed](#)]
15. Mohammadzadeh, N.; Gholamzadeh, M.; Saeedi, S.; Rezayi, S. The application of wearable smart sensors for monitoring the vital signs of patients in epidemics: A systematic literature review. *J. Amb. Intel. Hum. Comp.* **2020**; *1–15*, Online ahead of print. [[CrossRef](#)]
16. Pang, Y.; Yang, Z.; Yang, Y.; Ren, T.-L. Wearable Electronics Based on 2D Materials for Human Physiological Information Detection. *Small* **2019**, *16*, 1901124. [[CrossRef](#)]
17. Su, Y.; Ma, C.; Chen, J.; Wu, H.; Luo, W.; Peng, Y.; Luo, Z.; Li, L.; Tan, Y.; Omisore, O.M.; et al. Printable, Highly Sensitive Flexible Temperature Sensors for Human Body Temperature Monitoring: A Review. *Nanoscale Res. Lett.* **2020**, *15*, 200. [[CrossRef](#)] [[PubMed](#)]
18. Zhang, J.; Cao, Y.; Qiao, M.; Ai, L.; Sun, K.; Mi, Q.; Zang, S.; Zuo, Y.; Yuan, X.; Wang, Q. Human motion monitoring in sports using wearable graphene-coated fiber sensors. *Sens. Actuators A-Phys.* **2018**, *274*, 132–140. [[CrossRef](#)]
19. Zhao, T.; Fu, Y.; Sun, C.; Zhao, X.; Jiao, C.; Du, A.; Wang, Q.; Mao, Y.; Liu, B. Wearable biosensors for real-time sweat analysis and body motion capture based on stretchable fiber-based triboelectric nanogenerators. *Biosens. Bioelectron.* **2022**, *205*, 114115. [[CrossRef](#)] [[PubMed](#)]
20. Haug, W.B.; Drinkwater, E.J.; Cicero, N.J.; Barthell, J.A.; Chapman, D.W. The Impact of Dry-Land Sprint Start Training on the Short Track Speed Skating Start. *J. Strength Cond. Res.* **2019**, *33*, 544–548. [[CrossRef](#)] [[PubMed](#)]
21. Kim, K.; Kim, J.S.; Purevsuren, T.; Khuyagbaatar, B.; Lee, S.; Kim, Y.H. New method to evaluate three-dimensional push-off angle during short-track speed skating using wearable inertial measurement unit sensors. *Part I. Mech. Eng. H* **2019**, *233*, 476–480. [[CrossRef](#)] [[PubMed](#)]
22. Lu, Z.; Zhu, Y.; Jia, C.; Zhao, T.; Bian, M.; Jia, C.; Zhang, Y.; Mao, Y. A Self-Powered Portable Flexible Sensor of Monitoring Speed Skating Techniques. *Biosensors* **2021**, *11*, 108. [[CrossRef](#)] [[PubMed](#)]
23. Tomita, Y.; Iizuka, T.; Irisawa, K.; Imura, S. Detection of Movement Events of Long-Track Speed Skating Using Wearable Inertial Sensors. *Sensors* **2021**, *21*, 3649. [[CrossRef](#)] [[PubMed](#)]
24. Ji, Q.; Yang, X.J. Real-time eye, gaze, and face pose tracking for monitoring driver vigilance. *Real-Time Imaging* **2002**, *8*, 357–377. [[CrossRef](#)]
25. Liu, G.J.; Tang, X.L.; Cheng, H.D.; Huang, J.H.; Liu, J.F. A novel approach for tracking high speed skaters in sports using a panning camera. *Pattern Recogn.* **2009**, *42*, 2922–2935. [[CrossRef](#)]
26. Zhou, C.; Ren, D.C.; Zhang, X.Y.; Yu, C.G.; Ju, L.K. Human Position Detection Based on Depth Camera Image Information in Mechanical Safety. *Adv. Math. Phys.* **2022**, *2022*, 9170642. [[CrossRef](#)]
27. Feng, Y.; Han, J.; Xu, M.; Liang, X.; Jiang, T.; Li, H.; Wang, Z.L. Blue Energy for Green Hydrogen Fuel: A Self-Powered Electrochemical Conversion System Driven by Triboelectric Nanogenerators. *Adv. Energy Mater.* **2022**, *12*, 2103143. [[CrossRef](#)]
28. Fan, F.-R.; Tian, Z.-Q.; Wang, Z.L. Flexible triboelectric generator! *Nano Energy* **2012**, *1*, 328–334. [[CrossRef](#)]
29. Wen, Z.; Yang, Y.; Sun, N.; Li, G.; Liu, Y.; Chen, C.; Shi, J.; Xie, L.; Jiang, H.; Bao, D.; et al. A Wrinkled PEDOT:PSS Film Based Stretchable and Transparent Triboelectric Nanogenerator for Wearable Energy Harvesters and Active Motion Sensors. *Adv. Funct. Mater.* **2018**, *28*, 1803684. [[CrossRef](#)]
30. Xie, Z.; Zeng, Z.; Wang, Y.; Yang, W.; Xu, Y.; Lu, X.; Cheng, T.; Zhao, H.; Wang, Z.L. Novel sweep-type triboelectric nanogenerator utilizing single freewheel for random triggering motion energy harvesting and driver habits monitoring. *Nano Energy* **2020**, *68*, 104360. [[CrossRef](#)]
31. Zeng, Y.; Xiang, H.; Zheng, N.; Cao, X.; Wang, N.; Wang, Z.L. Flexible triboelectric nanogenerator for human motion tracking and gesture recognition. *Nano Energy* **2022**, *91*, 106601. [[CrossRef](#)]
32. Zhu, Y.; Sun, F.; Jia, C.; Zhao, T.; Mao, Y. A Stretchable and Self-Healing Hybrid Nano-Generator for Human Motion Monitoring. *Nanomaterials* **2022**, *12*, 104. [[CrossRef](#)] [[PubMed](#)]
33. Kim, M.P.; Kim, Y.-R.; Ko, H. Anisotropic silver nanowire dielectric composites for self-healable triboelectric sensors with multi-directional tactile sensitivity. *Nano Energy* **2022**, *92*, 106704. [[CrossRef](#)]
34. Li, S.; Zhao, Z.; Liu, D.; An, J.; Gao, Y.; Zhou, L.; Li, Y.; Cui, S.; Wang, J.; Wang, Z.L. A Self-Powered Dual-Type Signal Vector Sensor for Smart Robotics and Automatic Vehicles. *Adv. Mater.* **2022**, *34*, 2110363. [[CrossRef](#)] [[PubMed](#)]
35. Li, Y.; Chen, Z.; Zheng, G.; Zhong, W.; Jiang, L.; Yang, Y.; Jiang, L.; Chen, Y.; Wong, C.-P. A magnetized microneedle-array based flexible triboelectric-electromagnetic hybrid generator for human motion monitoring. *Nano Energy* **2020**, *69*, 104415. [[CrossRef](#)]
36. Xi, Y.; Hua, J.; Shi, Y. Noncontact triboelectric nanogenerator for human motion monitoring and energy harvesting. *Nano Energy* **2020**, *69*, 104390. [[CrossRef](#)]

37. He, H.; Zeng, H.; Fu, Y.; Han, W.; Dai, Y.; Xing, L.; Zhang, Y.; Xue, X. A self-powered electronic-skin for real-time perspiration analysis and application in motion state monitoring. *J. Mater. Chem. C* **2018**, *6*, 9624–9630. [[CrossRef](#)]
38. Zhou, Q.; Wang, B.; Gao, A.; Xu, W.; Zhou, K.; Pan, J.; Meng, G.; Pan, C.; Xia, F. Solution-Tube-Based Volume Effect Triboelectric Nanogenerator with Salt and pH Sensitivity. *Adv. Funct. Mater.* **2022**; 2209100, early view. [[CrossRef](#)]
39. Wei, Y.; Zhang, B.F.; Zhang, C.G.; Ou, Y.; Liu, Y.B.; He, L.X.; Zhou, L.L.; Zhao, Z.H.; Wang, J.; Wang, Z.L. Anaconda-shaped spiral multi-layered triboelectric nanogenerators with ultra-high space efficiency for wave energy harvesting. *One Earth* **2022**, *5*, 1055–1063.
40. Ko, H.-J.; Kwon, D.-S.; Pyo, S.; Kim, J. Curved flap array-based triboelectric self-powered sensor for omnidirectional monitoring of wind speed and direction. *Nano Energy* **2022**, *102*, 107717. [[CrossRef](#)]
41. Liu, R.; Li, M. A textile-based triboelectric nanogenerator for long jump monitoring. *Mater. Technol.* **2022**, *37*, 2360–2367. [[CrossRef](#)]
42. Shao, Y.; Zhou, F.; Wang, F. A Triboelectric Sensor with a Dual Working Unit for Race Walking Motion Monitoring. *J. Electron. Mater.* **2022**, *51*, 3569–3578. [[CrossRef](#)]
43. Sardana, S.; Kaur, H.; Arora, B.; Aswal, D.K.; Mahajan, A. Self-Powered Monitoring of Ammonia Using an MXene/TiO₂/Cellulose Nanofiber Heterojunction-Based Sensor Driven by an Electrospun Triboelectric Nanogenerator. *ACS Sens.* **2022**, *7*, 312–321. [[CrossRef](#)] [[PubMed](#)]
44. Fang, Y.; Zou, Y.; Xu, J.; Chen, G.; Zhou, Y.; Deng, W.; Zhao, X.; Roustaei, M.; Hsiai, T.K.; Chen, J. Ambulatory Cardiovascular Monitoring Via a Machine-Learning-Assisted Textile Triboelectric Sensor. *Adv. Mater.* **2021**, *33*, 2104178. [[CrossRef](#)] [[PubMed](#)]
45. Kim, J.-N.; Lee, J.; Lee, H.; Oh, I.-K. Stretchable and self-healable catechol-chitosan-diatom hydrogel for triboelectric generator and self-powered tremor sensor targeting at Parkinson disease. *Nano Energy* **2021**, *82*, 105705. [[CrossRef](#)]
46. Li, R.; Wei, X.; Xu, J.; Chen, J.; Li, B.; Wu, Z.; Wang, Z.L. Smart Wearable Sensors Based on Triboelectric Nanogenerator for Personal Healthcare Monitoring. *Micromachines* **2021**, *12*, 352. [[CrossRef](#)] [[PubMed](#)]
47. Su, Y.; Chen, G.; Chen, C.; Gong, Q.; Xie, G.; Yao, M.; Tai, H.; Jiang, Y.; Chen, J. Self-Powered Respiration Monitoring Enabled by a Triboelectric Nanogenerator. *Adv. Mater.* **2021**, *33*, 2101262. [[CrossRef](#)]
48. Yi, F.; Zhang, Z.; Kang, Z.; Liao, Q.; Zhang, Y. Recent Advances in Triboelectric Nanogenerator-Based Health Monitoring. *Adv. Funct. Mater.* **2019**, *29*, 1808849. [[CrossRef](#)]
49. Zhao, P.F.; Soin, N.; Prashanthi, K.; Chen, J.K.; Dong, S.R.; Zhou, E.P.; Zhu, Z.G.; Narasimulu, A.A.; Montemagno, C.D.; Yu, L.Y.; et al. Emulsion Electrospinning of Polytetrafluoroethylene (PTFE) Nanofibrous Membranes for High-Performance Triboelectric Nanogenerators. *ACS Appl. Mater. Inter.* **2018**, *10*, 5880–5891. [[CrossRef](#)]
50. Zhou, H.; Wang, H.X.; Shao, H.; Lin, T.; Xu, H.X.; Niu, H.T. Super-robust self-healing superhydrophobic coating with triboelectricity induced liquid self-repellency. *Mater. Des.* **2021**, *211*, 110145. [[CrossRef](#)]
51. Bai, Y.; Han, C.B.; He, C.; Gu, G.Q.; Nie, J.H.; Shao, J.J.; Xiao, T.X.; Deng, C.R.; Wang, Z.L. Washable Multilayer Triboelectric Air Filter for Efficient Particulate Matter PM_{2.5} Removal. *Adv. Funct. Mater.* **2018**, *28*, 1706680. [[CrossRef](#)]